Regular Article

Magnetically controllable Pickering emulsion prepared by a reduced graphene oxide-iron oxide composite

Kun-Yi Andrew Lin [a,*], Hongta Yang [b], Camille Petit [c], Wei-der Lee [a]

[a] *Department of Environmental Engineering, National Chung Hsing University, Taichung, Taiwan, ROC*
[b] *Department of Chemical Engineering, National Chung Hsing University, 250 Kuo-Kuang Road, Taichung, Taiwan, ROC*
[c] *Department of Chemical Engineering, Imperial College London, South Kensington Campus, Exhibition Road, London SW7 2AZ, UK*

A B S T R A C T

Pickering emulsions stabilized by graphene oxide (GO) have attracted much attention owing to the unique 2-D structure and amphiphilic surface properties of GO. On the other hand, investigations on reduced GO (RGO) to prepare Pickering emulsions are still limited, especially for water-in-oil (W/O) emulsions. Considering growing interests for directing Pickering emulsions to a specific location, it is necessary to embed Pickering emulsions with responsiveness upon external driving forces such as magnetic fields. To that end, we developed magnetically responsive RGO (denoted as "MRGO") and used MRGO to prepare W/O Pickering emulsions. MRGO was synthesized by decorating iron oxide nanoparticles on the surface of RGO and characterized by SEM, EDS, TEM, FT-IR, Raman, XRD and SQUID. MRGO Pickering emulsion (MRGO-PE) was prepared by suspending MRGO sheets in dodecane and mixing with water vigorously. The amount of MRGO added to prepare MRGO-PE is related to the size distribution of the droplets of MRGO-PE and the relationship can be well-described using a mass balance model. The motion of droplets of MRGO-PE under an external magnetic field is demonstrated. We also investigated the adsorptive property of MRGO-PE by evaluating the removal of Nile Red dye from dodecane. The results shows that the dye removal by MRGO-PE is not just achieved by MRGO layer of MRGO-PE but also by water encapsulated by MRGO. Owing to their magnetic property, MRGO-PE can be utilized as a magnetically-controlled carrier which can preserve and transport to specific locations certain compounds.

© 2014 Elsevier Inc. All rights reserved.

1. Introduction

Emulsions stabilized by solid particles are generally referred to Pickering emulsions [1]. Unlike emulsions stabilized by organic surfactants, Pickering emulsions possess many advantageous properties, including low toxicity [2], low cost [2], irreversible adsorption [3–6], self-assembly capability [7–10], improved stability [11], etc. These properties render Pickering emulsions intriguing in both fundamental research fields and in industry [3].

Among solid materials in Pickering emulsions, carbonaceous materials appear to be one of the most attractive ones owing to their mechanical and physical properties [12–15]. Up to date, there have been several examples of Pickering emulsions prepared by carbonaceous materials, including carbon nanotubes (CNTs) [13,16,17], graphene oxide (GO) [18–24], and GO-derived materials [15,25]. Pickering emulsions stabilized by GO have drawn significant attention owing to the unique 2-D structure and

amphiphilic surface properties of GO [19,20]. Indeed, GO, which is obtained by oxidation of graphite, exhibits several types of hydrophilic oxygen-containing groups on the surface and the basal planes of the graphene layers. Factors affecting GO-stabilized Pickering emulsions were also examined in detail, including sonication time, GO concentration, pH of aqueous solution, oil/water ratio, etc. [19,20,23]. While GO-stabilized Pickering emulsions have been extensively explored, studies reporting the use of reduced GO (RGO) in Pickering emulsions are still limited [19]. It has been revealed that more hydrophilic particles tend to stabilize oil-in-water (O/W) emulsions whereas more hydrophobic particles tend to stabilize water-in-oil (W/O) emulsion [19]. Therefore, the less hydrophilic RGO is expected to improve stability of W/O emulsions which are important to applications in drug delivery [4,26–29], cosmetic preparation [30,31] as well as food processing [32].

On the other hand, as the interest on manipulating Pickering emulsion droplets is growing, several studies have used magnetic nanoparticles to prepare Pickering emulsions [11,33–35]. This concept of magnetically-responsive liquid–liquid Pickering emulsion is also applied to air-air emulsions, so-called Pickering foams

* Corresponding author.
  E-mail address: linky@nchu.edu.tw (K.-Y.A Lin).

[5,36–47] and further extended to prepare liquid marbles (i.e., a liquid droplet encapsulated by solid particles in the air phase) [39,48–62]. Considering the increasing demand for developing magnetically-responsive and controllable Pickering emulsions, we proposed to develop a magnetically responsive materials based on RGO (denoted as "MRGO") to be used in Pickering emulsions, especially W/O emulsions. MRGO was synthesized by functionalizing RGO with magnetic iron oxide nanoparticles (ION). MRGO was characterized by Scanning Electronic Microscopy (SEM), Energy Dispersive X-ray Spectrometry (EDS) and Transmission Electronic Microscopy (TEM) to investigate its morphology and chemical composition. FT-IR and Raman spectroscopic analyses of MRGO were performed to examine MRGO's surface chemistry and conjugated carbon structures. X-ray Diffraction was also used to characterize the crystalline structure of MRGO. Since MRGO is a magnetic material, magnetization of MRGO was measured and compared to that of its precursor material, ION. MRGO Pickering emulsion (MRGO-PE) was prepared by first obtaining a suspension of MRGO sheets in oil (i.e., dodecane) and then mixing with water. We also investigated the relationship between the average size of droplets of MRGO-PE and the mass of MRGO as well as the kinetics of adsorption of MRGO to the surface of water droplets. The motion of droplets of MRGO-PE under an external magnetic field was demonstrated and the adsorptive property of MRGO-PE was also examined by evaluating the removal of a dye from dodecane.

2. Experimental

2.1. Materials and methods

All commercially available chemicals and solvents were used as received without further purification unless otherwise stated. The chemicals involved in this study include: Graphite (Showa Chemicals, Japan), iron sulfate Fe(SO$_4$) (Merck, Germany), sodium borohydride NaBH4 (Sigma–Aldrich, USA), Nile Red dye (Sigma–Aldrich, USA), glucose (Ferak, Germany), and dodecane (Tedia, USA). For all experiments/analyses involving water, deionized (D.I.) water exhibiting less than 18.0 MΩ cm was used. All other chemicals used in this study were analytical grade, purchased from commercial chemicals suppliers.

2.2. Synthesis of MRGO

GO was prepared by oxidation of natural graphite powder according to the modified Hummers' method [63]. MRGO was synthesized according to the scheme shown in Fig. 1(a) [64]. In brief, 200 mg of Fe(SO$_4$) was dissolved in 10 ml of D.I. water and the resulting solution was then added dropwise to 10 ml of ethanol containing 40 mg of NaOH to form "Solution A". Next, 200 mg of

GO was added to 100 ml of D.I. water and the suspension was sonicated for 30 min followed by vigorous stirring for 1 h. Glucose (200 mg) and 2 ml of ammonium hydroxide were then added to the GO suspension to obtain "Solution B". Solution A was added dropwise to Solution B while stirring. The new mixture was stirred for 30 min to ensure that GO was evenly dispersed. Subsequently, the mixture was poured into a Teflon-lined autoclave and heated at 160 °C for 4 h to reduced GO to RGO and decorate iron oxide nanoparticles (ION) on the surface of RGO. The product was washed with ethanol and D.I. water repeatedly and then dried at 90 °C for 24 h to obtain black-color MRGO, indicating that brownish GO had been converted to RGO. For comparison purposes, pure ION were also prepared using the above method without addition of GO. Similarly, reduced graphene oxide (RGO) was prepared according to a reported procedure using sodium borohydride (NaBH$_4$) [65].

2.3. Characterization of MRGO

The morphology of the as-synthesized MRGO was characterized using a Field Emission SEM (JEOL JSM-6700, Japan) and a Transmission Electronic Microscopy (JEOL JEM-2010, Japan). Absorption infrared (IR) spectroscopic analysis of MRGO was conducted using an infrared spectrometer (4100, Jasco, Japan) and the structures of conjugated carbon bonds of MRGO and precursor materials were analyzed by a Raman spectrometer (Nanofinder 30 R., Tokyo Instruments Inc., Japan). The powder X-ray diffraction patterns (PXRD) of MRGO and precursor materials were obtained using an X-ray diffractometer (PANalytical, the Netherlands) with copper as an anode material (40 mA, 45 kV). Magnetization of MRGO and ION were measured using a Superconducting Quantum Interference Device (SQUID) Vibrating Sample Magnetometer (Quantum Design MPMS SQUID VSM, USA) at 27 °C.

2.4. Preparation of MRGO-based Pickering Emulsion (MRGO-PE)

The preparation of MRGO-PE can be visualized using the scheme shown as Fig. 1(b). Firstly, a certain mass of MRGO, M_{MRGO}, was added to 20 ml of dodecane in a 30-ml polyethylene sample vial. The resulting suspension was sonicated for at least 10 min to exfoliate and disperse MRGO. Next, 0.5 g of D.I. water was added to the suspension and water in the sample vial formed a big droplet and settled in the bottom of the vial. The vial containing the mixture of MRGO, water, and dodecane was then placed on an orbital shaker to shake for 3 min at 300 rpm. During the vigorous shaking, the big droplet of water broke into smaller droplets which were encapsulated and stabilized by MRGO to form MRGO-PE. In this study, a series of MRGO-PE were prepared with various M_{MRGO} and a fixed mass of water, M_{water}. To distinguish MRGO-PE with
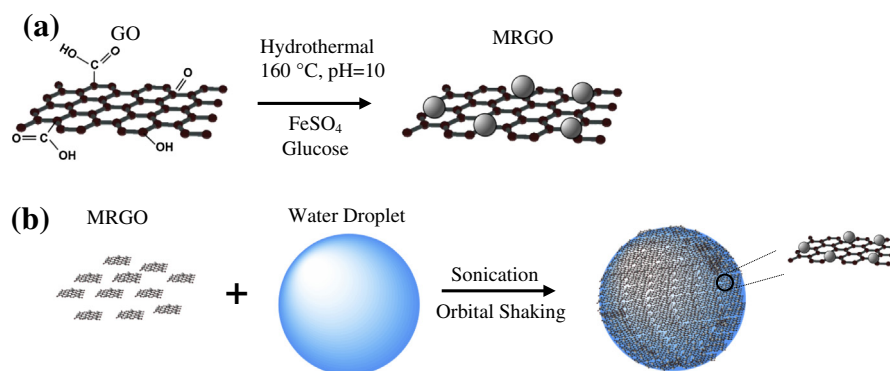
Fig. 1. Schematics for (a) the synthesis of magnetically responsive RGO (MRGO) and (b) the preparation of Pickering emulsion stabilized by MRGO (MRGO-PE).

various amounts of MRGO, a ratio of M_{MRGO} to M_{water} was adopted and denoted as "α". The values of α were selected from 0.0075 to 0.036 to represent low and high concentrations of MRGO in dodecane respectively. Droplet sizes of MRGO-PE were visualized and determined using a Nikon microscope (Alphaphot) equipped with a digital camera.

To estimate the coverage fraction of MRGO on the droplet, a water droplet was added to MRGO suspension and shaken. After a certain shaking time, the droplet covered by MRGO sheets was removed from the suspension and placed into clean dodecane under the microscope (Carl Zeiss microscope (Axiovert 200) equipped with a CCD camera) to visualize surface of the droplet. The as-obtained image was then compared with the pristine water droplet to quantify the area which had been covered by MRGO sheets. The coverage fraction was the ratio of the area covered by MRGO over the total area of the analyzed region. This was conducted using the image processing and analysis software "Image J" which is developed by National Institute of Health, USA.

2.5. Movement of MRGO-Pickering emulsion under a Magnetic field

Motion of MRGO-PE under a magnetic field was demonstrated by first placing three droplets of MRGO-PE with different sizes (0.6, 1.2, and 1.5 mm in diameter) in dodecane. Next, a permanent Neodymium magnet was used to draw these three droplets of MRGO-PE to a certain direction. The motion was visualized and recorded using a digital camera (Canon SX500IS).

2.6. Adsorption of Nile Red dye to MRGO-PE

The adsorptive properties of MRGO-PE were investigated for the removal of Nile Red dye from dodecane. MRGO-PE of $\alpha = 0.01$ was first prepared in a polyethylene vial. Nile Red dye in dodecane was then added to the MRGO-PE to reach a concentration of 20 mg L^{-1}. The mixture of MRGO-PE and Nile Red dye was immediately placed on the orbital shaker at 300 rpm at the ambient temperature for a certain time. After the adsorption, since MRGO-PE tended to settle down in the vial, the supernatant dodecane was collected to analyze the remaining concentration of Nile Red dye. The concentration of Nile Red dye in dodecane was determined using a UV–Vis spectrophotometer (ChromeTech CT-2200, Taiwan) with a calibration curve established by known concentrations of Nile Red dye in dodecane. In comparison with the adsorption capacity of MRGO-PE, MRGO alone was also used to adsorb Nile Red dye as MRGO-PE being tested. Finally, the stability of dye-containing MRGO-PE was tested by placing a droplet of the dye-containing MRGO-PE next to droplets of D.I. water, salt-containing water, and dye-containing water, respectively, to observe whether any breakages of MRGO-PE occurred in contact with these droplets.

3. Results and discussion

3.1. Characterization of MRGO

3.1.1. Morphology of MRGO

SEM and TEM were taken in order to characterize the structure of MRGO. As seen in Fig. 2(a), MRGO sheets look rather disordered and entangled. Since MRGO powders were not exfoliated to form MRGO sheets prior to the sonication process, the bulk MRGO powder was fluffy. However monolayers of MRGO can still be observed on the edge of the bulk MRGO powder. To examine the chemical composition of the as-synthesized MRGO, EDS was used and the results are summarized in Fig. 2(b). The composition analysis reveals that MRGO mainly consisted of carbon, oxygen and iron and their corresponding atomic percentages are 65.61%, 29.40%

and 5.00%, respectively. The existence of iron indicates that iron oxide nanoparticles were successfully decorated on the surface of RGO.

To visualize single MRGO sheets, MRGO sheets were exfoliated using sonication and the obtained material was analyzed by TEM (Fig. 3(a)). The TEM image reveals that the size of MRGO sheets was in the range of 200–400 nm and the MRGO sheets were also decorated with well-dispersed and uniform ION. Fig. 3(b) shows the size distribution of ION on MRGO sheets and the sizes were concentrated in the range of 2–13 nm. The histogram plot was fitted using a Gaussian distribution to determine its mean value and standard deviation which were 6.5 and 3.4 nm respectively. The size of ION was comparable to the reported value obtained by a similar synthesis procedure [64].

3.1.2. FT-IR spectroscopic analyses

To characterize the surface chemistry of MRGO, the FT-IR spectrum of MRGO was taken and compared to those of the precursor materials. Fig. 4 shows the FT-IR spectra of graphite, GO, RGO, and MRGO. As expected, graphite's spectrum is rather featureless. However, after graphite was oxidized to form GO, GO exhibited several well-pronounced bands at 1040 cm^{-1} (C—O—C), 1220 cm^{-1} (C—O), 1415 cm^{-1} (C—O—H), 1620 cm^{-1} (C=C), 1732 cm^{-1} (C=O), 3400 cm^{-1} (O—H) [66,67]. As expected, the intensities of these bands decreased after reduction of GO, especially the bands at 1040 cm^{-1} (C—O—C) and 1220 cm^{-1} (C—O). Similarly, the intensities of the bands at 1040 and 1220 cm^{-1} also decreased significantly on the spectrum of MRGO, indicating the effective reduction of GO for that material as well. In addition to the characteristic bands of RGO, MRGO also exhibited an intense band at 600 cm^{-1}, which can be attributed to lattice adsorption of iron oxides present on the surface of MRGO [68], confirming that ION were successfully dispersed onto MRGO sheets.

3.1.3. Raman spectroscopic analyses

Raman spectroscopy was used to characterize the structure of conjugated carbon bonds in MRGO and the precursor materials (i.e., GO and RGO). Their Raman spectra are shown in Fig. 5. Raw graphite exhibited two characteristic bands: a sharp band at 1580 cm^{-1}, so-called "G band" and a relatively small band at 1355 cm^{-1}, so-called "D band". The G band is attributed to the doubly degenerate zone center E_{2g} mode derived from the structural integrity of sp^2-hybridized carbon atoms [69]. On the other hand, the D band is linked to disorder sp^2-hybridized carbon atoms which consist of vacancies, impurities, and symmetry-breaking defects [69]. After raw graphite was oxidized and exfoliated to form GO, the intensity of the D band of GO increased and exhibited a broader shape than that of raw graphite due to the sp^3 amorphous carbons derived from oxidation. Additionally, the G band of GO noticeably shifted to higher frequencies (blue shift) [70] compared to that of graphite. A trend similar to that of graphite was found for RGO (and MRGO) due to the less ordered carbon atoms and defects of RGO sheets compared to graphite [71]. The extent of carbon-containing defects in graphitic materials can be determined using an intensity ratio of the D band to the G band (I_D/I_G) [72]. The I_D/I_G ratios for raw graphite, GO, RGO and MRGO were 0.223, 0.883, 1.053 and 1.129, respectively. As raw graphite was oxidized to GO and further converted to RGO and MRGO, the I_D/I_G ratio continued to increase, indicating that GO, RGO and MRGO all possessed fewer graphitized structures than raw graphite.

3.1.4. XRD spectroscopic analyses

Fig. 6 shows the XRD patterns of GO, RGO, ION, and MRGO. GO exhibited a characteristic peak at $2\theta = 11.5°$, corresponding to an interlayer spacing of 7.7 Å (d_{002}) for the stacked GO sheets. As
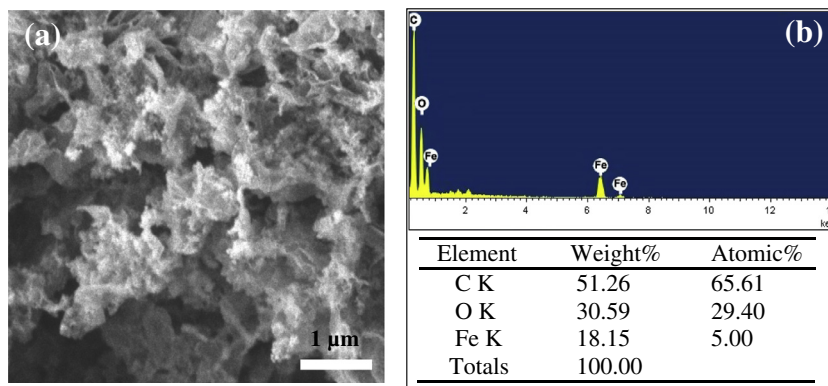
Fig. 2. Morphology and chemical composition of the as-synthesized bulk MRGO: (a) SEM image and (b) EDS analysis of MRGO.

Element	Weight%	Atomic%
C K	51.26	65.61
O K	30.59	29.40
Fe K	18.15	5.00
Totals	100.00	
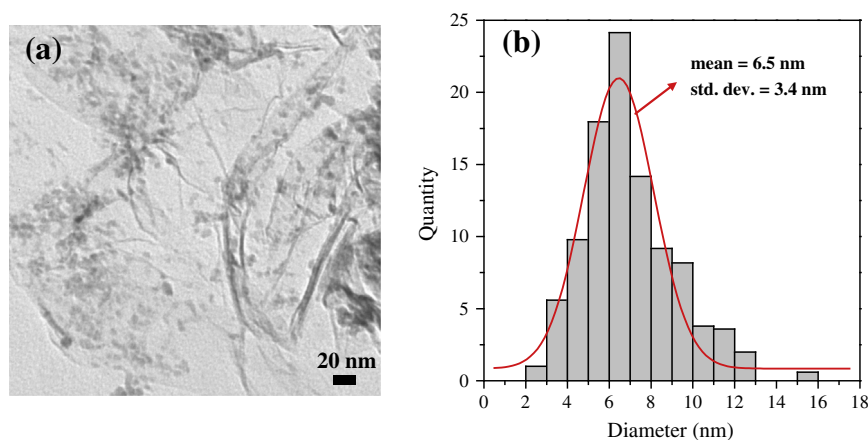
Fig. 3. Morphology of MRGO sheet: (a) TEM image of MRGO and (a) size distribution of iron oxide nanoparticle (ION) present on the surface of MRGO.
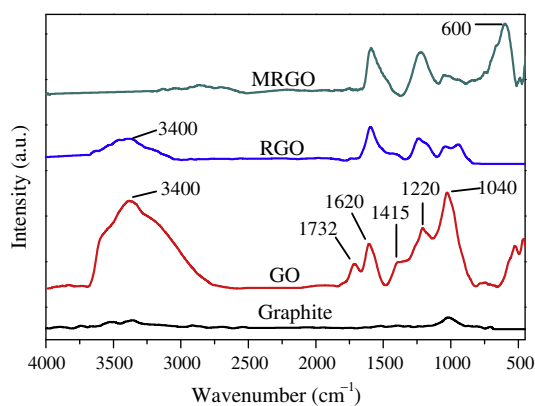
Fig. 4. FT-IR spectra of Graphite, GO, RGO and MRGO.
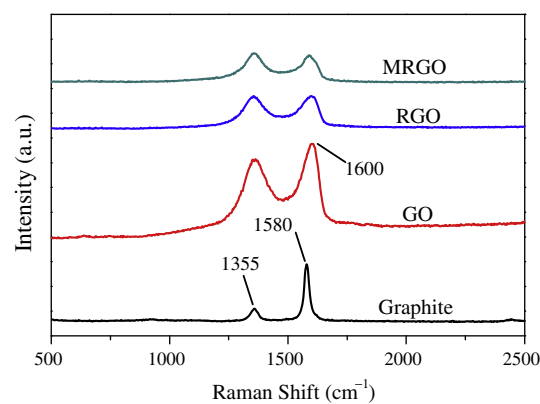
Fig. 5. Raman spectra of Graphite, GO, RGO and MRGO.

expected, the interlayer space is increased compared to that of graphite because of the presence of oxygen-containing groups as well as the atomic-scale roughness derived from structural defects (i.e., sp^3 bonding) [64,73]. XRD patterns of RGO showed a broad peak $(0\,0\,2)$ at the range $2\theta = 23$–$26°$, corresponding to $d_{002} = {\sim}3.5$ Å. The substantial change in d_{002} from 7.7 to 3.5 Å is due to the elimination of the oxygen-containing groups [73,74]. To examine the structure of ION on MRGO, ION alone was also examined using XRD.

It was found that ION consisted of γ-Fe_2O_3 and Fe_3O_4. This could be deduced from the presence of the peaks at 36.52°, 62.64°, 43.52° and 53.54°, corresponding to $(3\,1\,1)$, $(4\,4\,0)$, $(4\,0\,0)$ and $(4\,2\,2)$ crystal

planes of γ-Fe_2O_3 (JCPDS 39-1346), and at 30.2°, 35.6°, 43.3°, 53.7°, 57.3° and 62.8°, corresponding to $(2\,2\,0)$, $(3\,1\,1)$, $(4\,0\,0)$, $(4\,2\,2)$, $(5\,1\,1)$ and $(4\,4\,0)$ crystal planes of Fe_3O_4 (JCPDS 19-0629). On the XRD pattern of MRGO, one can recognized the pattern of RGO (i.e., the peak at $2\theta = 23$–$26°$) and that of ION indicating that GO was reduced to form MRGO and that both γ-Fe_2O_3 and Fe_3O_4 were dispersed on the surface of the RGO sheets.

3.1.5. Magnetization of MRGO and ION

The magnetic properties of MRGO were also examined. Fig. 7 illustrates the magnetizations of MRGO and ION as a function of
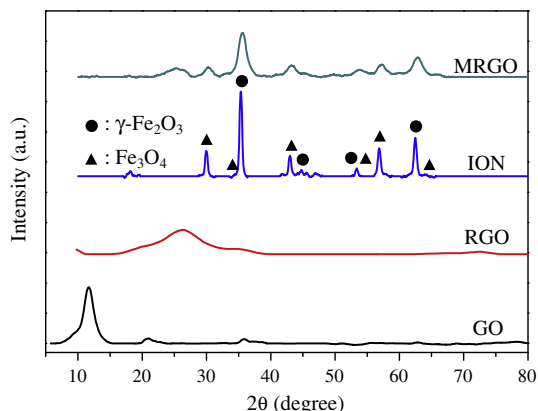
Fig. 6. XRD analyses of GO, RGO, ION and MRGO. The circle symbol (●) represents the XRD patterns of γ-Fe_2O_3 whereas the triangle symbol (▲) represents the patterns of Fe_3O_4 according to JCPDS.
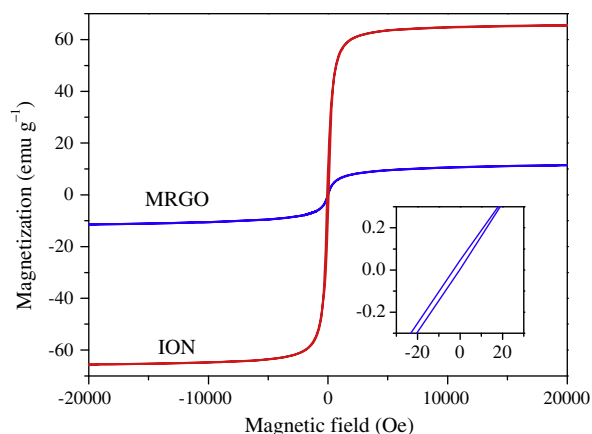
Fig. 7. Magnetization curves of MRGO and ION at 27 °C. The inset shows a negligible coercivity in MRGO.

magnetic field. Under a varying magnetic field, MRGO exhibited the superparamagnetic characteristic with negligible histeresis (see the inset of Fig. 7). Coercivity of MRGO was found to be only 3.46 (±0.3) Oe, indicating that MRGO were superparamagnetic with negligible remanence of magnetization. In addition, the saturation magnetization of MRGO was found to be 11.4 emu g^{-1} whereas that of ION was 65.0 emu g^{-1}. This difference was mainly attributed to the fact that MRGO only contained around 18 wt% of iron according to the EDS result discussed in the earlier section. Although the saturation magnetization of MRGO was smaller than that of ION, MRGO still exhibited high magnetic sensitivity which could be utilized in magnetically-controllable applications.

3.2. MRGO-based Pickering emulsion (MRGO-PE)

3.2.1. Formation of MRGO-PE

Preparation and formation of MRGO-PE was demonstrated in a sequence of pictures in Fig. S1 (see ESI†). Fig. S1(a) shows a vial containing colorless dodecane before MRGO was added to the vial. Once MRGO powder (0.005 g) was added to the vial and sonicated, MRGO was exfoliated and dispersed evenly in the vial to render the vial black color (Fig. S1(b), ESI†). Subsequently, 0.5 ml of water was added to the MRGO suspension which was shaken to break the large water droplet into small droplets. During the shaking process, these small water droplets were stabilized and encapsulated by MRGO to form MRGO-PE (Fig. S1(c), see ESI†). The supernatant of

the vial (Fig. S1(c)) also became relatively clear after the shaking process, indicating that MRGO were displaced from dodecane to the surface of the water. After decanting the as-prepared MRGO-PE to a rectangular dish (Fig. 8(a)), we observed that the original large droplet broke up into numerous mono-dispersed black small droplets, showing that droplets of MRGO-PE were stable. The layer of MRGO on the surface of water droplets protected the encapsulated water droplets and prevented them from coalescence. For comparison, ION was also used to prepare a Pickering emulsions using the same procedure for preparation of MRGO-PE. However, the mixture of dodecane, water and ION did not become a stable W/O Pickering emulsion using the preparation procedure. Instead, ION was dissolved in water to result in a large droplet as shown in Fig. 8(b). The same phenomenon was observed when GO, instead of MRGO, was used to prepare Pickering emulsion as shown in Fig. 8 (c). Fig. S2 (see ESI†) shows the contact angles of GO, ION and MRGO. The contact angles of GO and ION were found to be below 90°, whereas that of MRGO was 109°. Thus, the reason that using GO and ION could not form stable W/O Pickering emulsions was due to the highly hydrophilic surfaces of GO and ION. Since GO and ION both had oxygen-containing groups on their surfaces, these oxygen-containing groups (e.g., hydroxyl groups, carboxylic groups, epoxide groups, etc.) [19,75] rendered GO and ION highly hydrophilic. Consequently, GO and ION were fully wetted by water and therefore remained only in the phase of water [19]. In contrast, MRGO was not wetted by water, confirming that MRGO exhibited a less hydrophilic behavior which led MRGO to preferentially stay at the interface of water/dodecane.

3.2.2. Size distributions of MRGO-PE

Although water added to the vial was broken into a number of small droplets encapsulated by MRGO as shown in Fig. 8(a), a range of different sizes of droplets for MRGO-PE was still observed. These water droplets required encapsulation by MRGO to avoid coalescence, and therefore the amount of MRGO added to prepare the Pickering emulsion can be a critical parameter to control the size of the droplets. Therefore, we further varied the amount of MRGO added to prepare MRGO-PE while fixing the amount of water present in the system. A ratio "α" was used to express the ratio of the mass of MRGO, M_{MRGO}, to the mass of water, M_{water}. To obtain representative size distributions, at least triplicates of each MRGO-PE of a certain "α" value were prepared and the sizes of droplets were visualized using a microscope equipped with a digital camera. The droplets images were then analyzed using the image processing and analysis software "Image J", to determine the size distribution. In this study, α was varied from 0.0075 to 0.036. Fig. 9 shows histogram plots of size distributions for α = 0.0075, 0.010, 0.015, 0.025, 0.030 and 0.036. In Fig. 9(a), it can be seen that when α is 0.0075, the size of the droplets ranges from 0.25 to 5 mm. The size distribution was fitted using a Gaussian function to estimate the average size which was found to be 2.00 (±0.16) mm. However, when α was increased to 0.010, the size distribution of droplets narrowed down (Fig. 9(b)) and a dominant size of 1.7 mm was noticed. In comparison with the average size of α = 0.0075, the average size for α = 0.010 was decreased to 1.64 (±0.12) mm, showing that, as expected, a higher amount of MRGO present in the system can result in smaller stable droplets of Pickering emulsions. When α was further increased to 0.015, the range of size distribution became narrower. In particular, the dominant size of droplets was shifted to a smaller value and the average size of droplets was found to be 1.07 (±0.08) mm. α was then increased to 0.025, resulting in a size distribution ranging from 0 to 1.75 mm. The average size of MRGO-PE was reduced to 0.63 (±0.08) mm. For α = 0.300 and 0.036, the ranges of size distribution were 0–1.25 mm. The average sizes for MRGO-PE of α = 0.300 and 0.036 were 0.49 (±0.08) and 0.47 (±0.08) mm, respectively. Since water added in
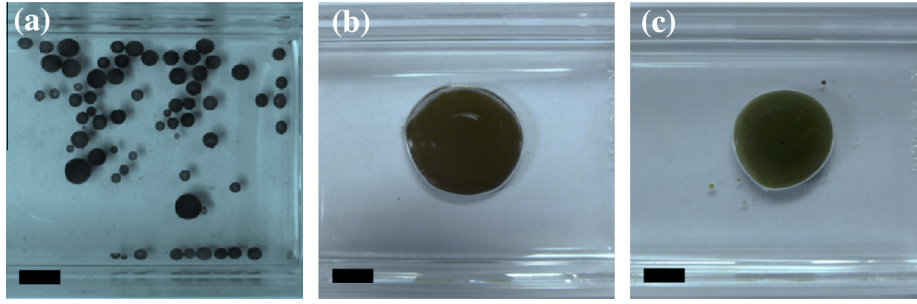
Fig. 8. Pictures of (a) MRGO and water in dodecane, (b) the mixture of ION and water in dodecane, and (c) the mixture of GO and water in dodecane, after the vigorous shaking process. The scale bar is 50 mm.
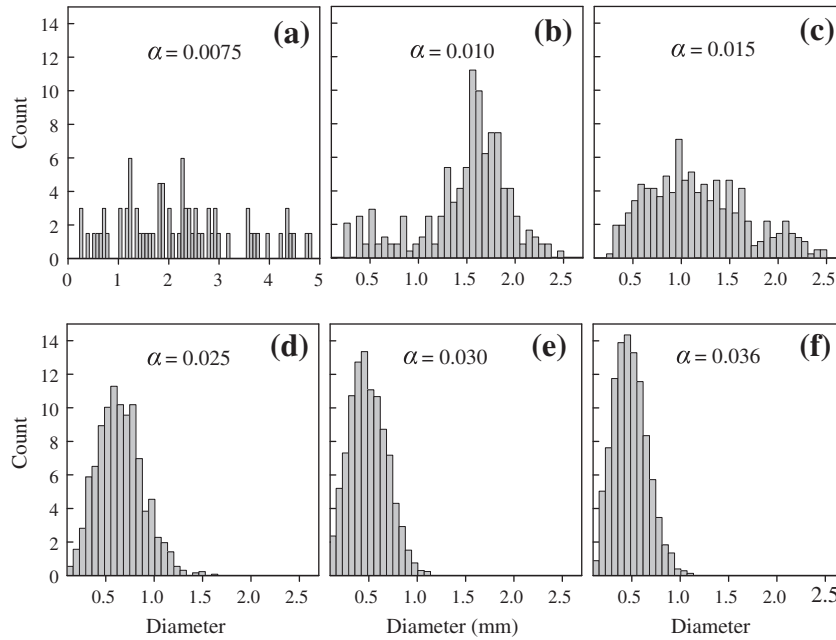
Fig. 9. Histogram plots of size distribution of droplets of MRGO-PE with different α values (normalized to 100 droplets in each case). α represents the mass ratio of the weight of MRGO, M_{MRGO}, over the weight of water, M_{water}.

the preparation of MRGO-PE was constant regardless of α, smaller droplets of MRGO-PE meant that a higher number of droplets formed after the shaking process during the preparation. These smaller droplets resulted in a much larger surface area for the same total water volume. In order to stabilize these small droplets, a higher amount of MRGO was required to encapsulate the surface of these MRGO-PE droplets and prevent them from coalescence. Therefore, there should be a relationship between the average size of droplets and the value of α. To model this relationship, the mass of water, M_{water}, was expressed as follows [13]:

$$M_{water} = \frac{\rho_{water} N \pi d^3}{6} \tag{1}$$

where ρ_{water} is the density of water and N is the number of water droplets present in MRGO-PE; d is the average diameter of droplets. On the other hand, the mass of MRGO, M_{MRGO}, was expressed as follows:

$$M_{MRGO} = \rho_{MRGO} N h \pi d^2 \theta \tag{2}$$

where ρ_{MRGO} is the density of MRGO and h is the average thickness of MRGO residing on the surface of water droplets to encapsulate the droplets. θ is the coverage fraction accounting for the ratio of the area covered by MRGO over the surface area of a water droplet.

Since α was defined as the ratio of M_{MRGO} to M_{water}, α could be expressed in the following equation:

$$\alpha = \frac{M_{MRGO}}{M_{water}} = \frac{\rho_{MRGO} N h \pi d^2 \theta}{\frac{\rho_{water} N \pi d^3}{6}} \tag{3}$$

Eq. (3) was rearranged to express the droplet diameter, d, as a function of ρ_{MRGO}, ρ_{water}, h, θ, and α (Eq. (4)).

$$d = 6 \frac{\rho_{MRGO}}{\rho_{water}} \frac{h}{\alpha} \theta \tag{4}$$

Since ρ_{MRGO} and ρ_{water} are the physical properties of MRGO and remain constant at a steady condition, the average diameter was proportional to the product of h, θ and α^{-1}. Here we assume that the average thickness of MRGO residing on the surface of water was constant. The coverage fraction, θ, was also expected to approach a constant value in the size range that we studied as the adsorption of MRGO sheets to the surface of the water droplet approached the equilibrium. This is because the curvature of the surface has minimal effect on the interfacial stability when the droplet size is larger than a few microns. Consequently, the average diameter should be inversely proportional to α (i.e., $d \propto \alpha^{-1}$). To examine this relationship, we plotted the average diameter of droplets as a function of α in Fig. 10. It must be noted that the error

bars in Fig. 10 are related to the standard deviations from the sets of three replicate measurements conducted to determine the average droplet size for each α value (Fig. 9 only show one set of measurements). It can be seen that an increase in α results in a decrease in the average droplet diameter. These data points were then fitted using the non-linear regression with a power function. The fitting curve was plotted as the red line in Fig. 10 and the equation of the fitting curve was $d = 0.015\,\alpha^{-1.00(\pm 0.09)}$ ($R^2 = 0.984$) confirming the inversely proportional relationship between the average diameter and α. The coefficient, 0.015, was directly proportional to the product of ρ_{MRGO}, ρ_{water}^{-1}, θ and h. To estimate the coverage fraction of MRGO on the surface of water droplets, the adsorption kinetics of MRGO sheets to a droplet was investigated. The adsorption process can be visualized in Fig. 11 at different shaking times. Before contact with MRGO, the surface of a droplet of water was clear as shown in Fig. 11(a). After addition of MRGO and shaking, MRGO sheets started to reside on the surface of the droplet (Fig. 11(b) and (c)). To quantitatively determine the amount of MRGO covering the surface of the droplet, each image of the droplet at the different shaking times was analyzed by estimating the area covered with dark MRGO sheets. A coverage fraction was used to quantify the ratio of the area covered by MRGO sheets over the surface area of the water droplet. The coverage fraction as a function of the shaking time is depicted in Fig. 12. The coverage on the droplet rapidly increased as the shaking time increased and then reached equilibrium. Both the pseudo-first-order and the pseudo-second-order equations were tested to estimate the kinetic constants and the coverage fraction at equilibrium.

The pseudo-first-order equation can be expressed as follows:

$$\theta_t = \theta_e(1 - e^{-k_1 t}) \tag{5}$$

where θ_t and θ_e are the coverage fraction at time t and at equilibrium, respectively. k_1 (min^{-1}) is the rate constant for the pseudo first order equation. The pseudo-second-order equation can be described by the following equation:

$$\theta_t = \frac{k_2 \theta_e^2 t}{1 + k_2 \theta_e t} \tag{6}$$

where k_2 (g mg^{-1} min^{-1}) represents the rate constant for the pseudo second order equation. Fig. 12 illustrates the kinetic data fitted using the pseudo-first-order (the dash line) and the pseudo-second-order (the solid line) equations. Although the kinetic data can be fitted rather well by two linear lines of the pseudo-first-order and the pseudo-second-order equations, the pseudo-second-order
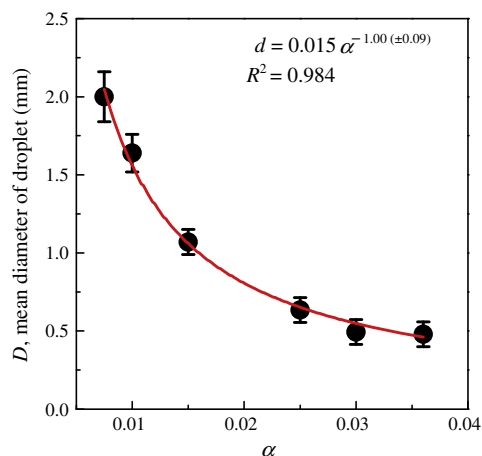
equation appears to be more satisfactory to describe the kinetic data. Table 1 summarizes the kinetic constants and the coverage fraction at equilibrium using these two equations. It can be seen that the latter one exhibits a higher correlation coefficient of 0.993, confirming that the pseudo-second-order is a better equation to represent the kinetic data. The coverage fraction at equilibrium estimated from the pseudo-second-order equation was 0.898, showing that 10% of the area of the droplet was not covered by MRGO.

As the coverage fraction at equilibrium was obtained and ρ_{MRGO} and ρ_{water} were constant at 25 °C and 1 atm, the coefficient of 0.015 could be used to estimate the average thickness, h. The particle density of MRGO, ρ_{MRGO}, was measured using a Pycnometer at 25 °C [76] and found to be 1.43 (± 0.24) g/cm^3. The density of water, ρ_{water}, was taken as 1.00 g/cm^3 under the experiments conditions. Thus, the thickness was then estimated using Eq. (4) and found to be 1.83 (± 0.45) μm.

3.3. Magnetic motion of different MRGO-PE

The magnetic properties of MRGO were examined in the earlier section and found that MRGO was ferromagnetic and sensitive under an external magnetic field. Since MRGO-PE is designed to exhibit magnetically responsive properties, it is also important to examine their motion under an external magnetic field. To visualize the motion of the droplets of MRGO-PE, three droplets of MRGO-PE with different sizes, 0.6, 1.2 and 1.5 mm in diameter, were prepared and lined up in dodecane as shown in Fig. 13(a). Once an external magnetic field was applied using the neodymium magnet, these three droplets of MRGO-PE started to move as shown in the sequential pictures in Fig. 13(b)–(e). During the motion, these three droplets were not broken or misshaped, showing the stability of emulsions under the magnetic field. Another noteworthy phenomenon was that the biggest droplet (i.e., 1.5 mm) was the first one to move, followed by the middle one and then the smallest one. This could be attributed to the different absolute amounts of MRGO residing on the surface of the droplets. Based on the estimated thickness and the density of MRGO, the weights of MRGO residing on these three droplets were 2.75×10^{-7} g, 11.00×10^{-7} g and 17.20×10^{-7} g for the droplets of 0.6, 1.2 and 1.5 mm in diameter, respectively. Different weights of MRGO layer residing on the surface of water droplets indicate different amounts of ION present. Therefore, this results in different degrees of magnetization under the same magnetic field, and thereby leads to the different response of the three droplets. To analyze their motion, a plot of distance traveled by the droplets away from the starting point as a function of time is displayed in Fig. 14. Interestingly, although the different droplets started to move at distinct times, their trajectory and motion were similar. All three droplets moved slowly in the beginning and then speeded up because the magnetic field strength became stronger as these droplets approached the magnet.

3.4. Adsorptive property of droplets of MRGO-PE: adsorption of Nile Red dye

When Pickering emulsions exist in the presence of other molecules, the interactions between the PE droplets and the molecules are critical to the stability as well as the adsorption property of PE droplets. As graphene and graphene oxide are proven as promising materials for adsorption applications [77,78], Pickering emulsion stabilized by MRGO was expected to act as an adsorbent system. Therefore, in this study, MRGO-PE was tested for sorption of an organic dye, i.e. Nile Red. Fig. 15 shows the adsorption capacity of MRGO-PE as a function of reaction time. The adsorption capacity was determined by the following equation (Eq. (7)):

Fig. 10. Correlation of the average diameter, d, of droplets of MRGO-PE with the α value.
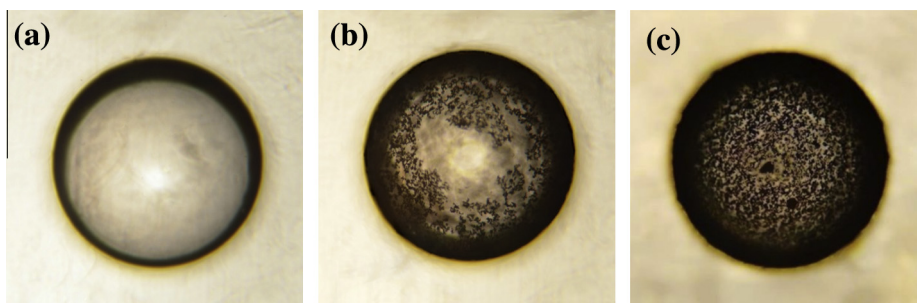
Fig. 11. Pictures of (a) water droplet in dodecane prior to contacting with MRGO (i.e., shaking time = 0), (b) MRGO starts to reside on the surface of the water droplet in contact with MRGO (the shaking time = 15 s), (c) the adsorption of MRGO on the surface of the water droplet approaches equilibrium (the shaking time = 120 s). The diameter of the droplet in the images is 1.5 mm.
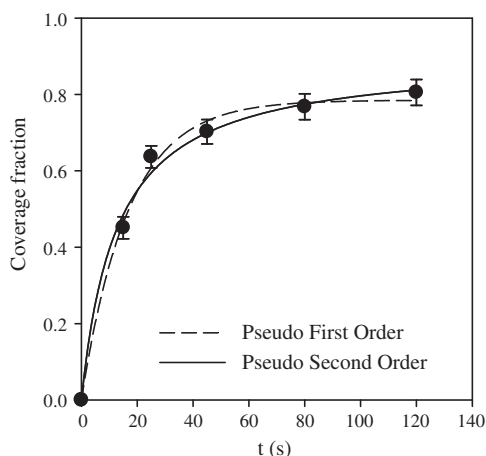
Fig. 12. Coverage fraction of a water droplet by MRGO as a function of shaking time at 25 °C and the kinetic analysis using the pseudo-first-order (dash line) and the pseudo-second-order (solid line) equations.

Table 1
Model parameters for the Pseudo first order (1) and Pseudo-second order (2) equations for the coverage kinetics of MRGO on the droplet. k_1 and k_2 are kinetic constants of the pseudo first order and the pseudo second order rate laws, respectively. R_1^2 and R_2^2 are the correlation coefficients. $\theta_{e,fitted}$ is the estimated coverage fraction at equilibrium using the kinetic models.

Condition	Pseudo-first-order			Pseudo-second-order		
	k_1 (min^{-1})	$\theta_{e,fitted}$	R_1^2	k_2 (g g^{-1} min^{-1})	$\theta_{e,fitted}$	R_2^2
25 °C	0.942	0.785	0.920	0.087	0.898	0.993

$$q_t = \frac{V(C_0 - C_t)}{m} \tag{7}$$

where q_t is the adsorption capacity at time t, V is the volume of the solution containing Nile Red dye. C_0 is the initial concentration of
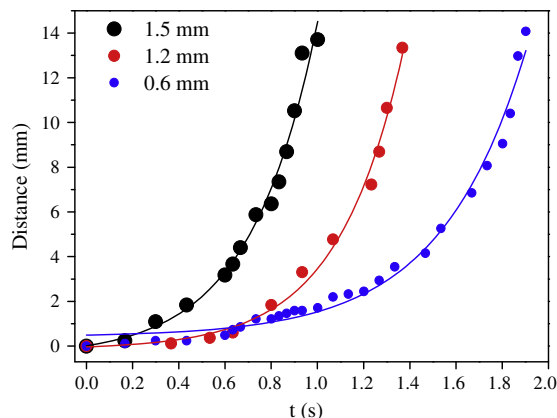
Fig. 14. The travel distance of these three droplets of MRGO-PE mentioned in Fig. 13 as a function of time after the magnetic field is applied.

Nile Red dye in dodecane and C_t is the concentration of Nile Red dye at the time t; m is the mass of MRGO added to the solution of dodecane. As seen in Fig. 15(a), MRGO-PE adsorbed Nile Red dye quickly in the beginning (i.e., 0–10 min) and then the adsorption increased slowly until reaching equilibrium after 20 min, indicating that Nile Red dye can be adsorbed to MRGO-PE and equilibrium existed between the continuous phase (i.e., dodecane) and the droplets (i.e., MRGO-PE). Since droplets of MRGO-PE consisted of MRGO and water, we also examined the adsorption capacity of MRGO for removal of Nile Red dye and the solubility of Nile Red dye in water individually. Fig. 15(a) reveals Nile Red dye is slightly soluble in water and that MRGO exhibited a strong affinity for Nile Red dye. Another interesting feature in Fig. 15(a) is that the kinetics of the dye adsorption in MRGO was faster than that in MRGO-PE. This was due to the fact that MRGO sheets were well-dispersed in dodecane when MRGO was used alone. In contrast, MRGO sheets were in
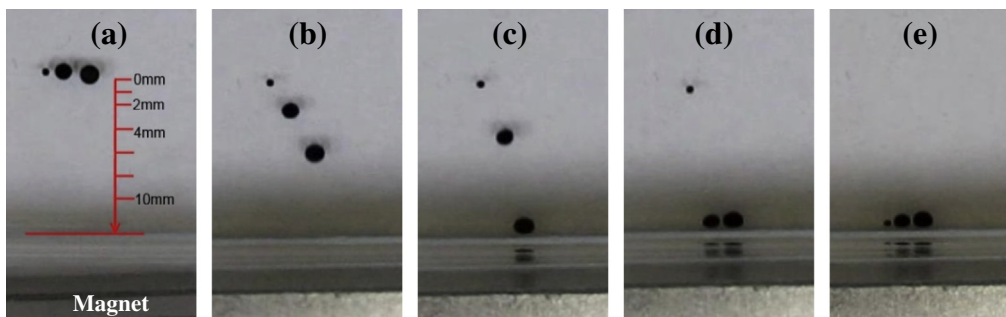
Fig. 13. Sequence of pictures showing the trajectory of droplets of MRGO-PE under an external magnetic field in dodecane. The sizes of three droplets shown above are 0.6 mm for the smallest one (to the left), 1.2 mm for the middle one, and 1.5 mm for the largest one (to the right). The neodymium magnet is placed at the bottom of the picture.
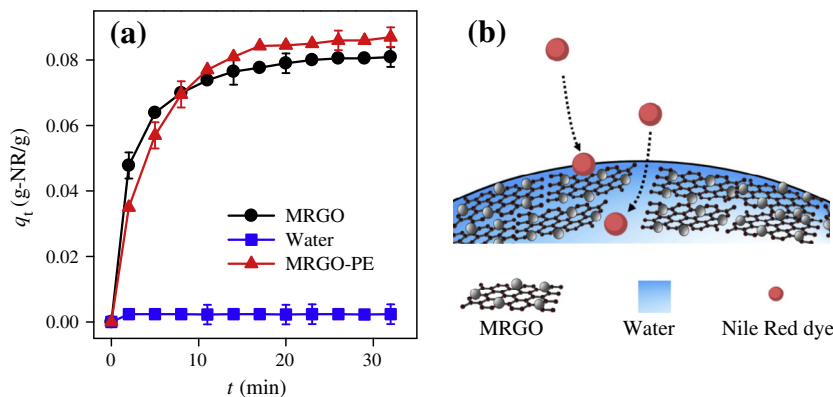
Fig. 15. Removal of Nile Red dye from dodecane using MRGO-PE, MRGO of the equivalent weight present in MRGO-PE, and water of the equivalent weight present in MRGO-PE: (a) kinetics of Nile Red dye removed using MRGO and MRGO-PE as well as Nile Red dye solubility in water as a function of time; (b) a proposed mechanism of Nile Red dye removed using MRGO-PE. The dye is adsorbed by the MRGO sheets residing on the surface of the water droplet and penetrates through the interface of water/dodecane not covered by MRGO sheets.

contact with the surface of the water droplets in MRGO-PE. Nevertheless, the dye adsorption capacity of MRGO-PE was noticeably higher than that of MRGO alone. The difference could be attributed to the amount of the dye being soluble in the water droplets. This interesting feature suggests that solutes can be adsorbed not only by the layer of MRGO residing on the surface of the droplets but also "captured" inside droplets of the discrete phase (i.e., water in this study) encapsulated by MRGO sheets. This mechanism is illustrated in Fig. 15(b). The proposed adsorption scenario is a hypothesis and further experiments, as for instance dual microscopic/spectroscopic techniques, could enable to validate or invalidate it. From the result of the adsorption of MRGO to the surface of the water droplets, we found that the coverage fraction of MRGO on the surface of water droplet was ∼90%. Thus, the dye could still be transferred from the oil phase to the water phase at the regions where MRGO sheets are not present. Fig. S3 (ESI†) also reveals that the droplet of MRGO-PE containing the dye did not break or coalesce in contact with a pure water droplet, a water droplet containing NaCl or a water droplet containing the same dye. This suggests that the droplet of MRGO-PE containing the dye was protected by the layer of MRGO and the dye can be preserved.

4. Conclusion

In this study, we have successfully prepared a composite of reduced graphene oxide and iron oxide nanoparticles, denoted as "MRGO". MRGO was decorated with spherical iron oxide nanoparticles of ∼10 nm (γ-Fe_2O_3 and Fe_3O_4) in diameter, which rendered MRGO magnetically responsive. MRGO Pickering emulsion (MRGO-PE) was prepared by first obtaining a suspension of MRGO sheets in dodecane and then mixing with water. By varying the amount of MRGO added to prepare MRGO-PE, the average size of the droplets of MRGO-PE also changed, indicating a specific relationship between the amount of MRGO and the average size of the droplets. We also examined the kinetics of MRGO adsorption to the surface of the water droplets, which seemed to follow a pseudo second order rate law. The motion of the droplets of MRGO-PE under an external magnetic field was also visualized and was found to be associated with the size of the droplet and the magnetic field strength. In addition, the adsorption properties of MRGO-PE were investigated for the removal of Nile Red dye from oil. The results indicated that the dye removal occurred via: (i) adsorption on the surface of the MRGO sheets and (ii) transfer to the water droplets owing to the fact that coverage of the water droplet is covered up to 90% by the MRGO sheets. The MRGO-PE

containing the dye did not break or coalesce in contact with bare water droplets. Thus, the magnetically responsive MRGO-PE can be utilized as a carrier to preserve certain compounds and transport to specific locations by the external magnetic field.

Appendix A. Supplementary material

Supplementary data associated with this article can be found, in the online version, at http://dx.doi.org/10.1016/j.jcis.2014.10.015.

References

[1] S.U. Pickering, Transactions 91 (1907) 2001.
[2] A.K.F. Dyab, H.A. Al-Lohedan, H.A. Essawy, A.I.A. Abd El-Mageed, F. Taha, J. Saudi Chem. Soc. 18 (2014) 610.
[3] E. Dickinson, Curr. Opin. Colloid Interface Sci. 15 (2010) 40.
[4] J. Frelichowska, M.-A. Bolzinger, J. Pelletier, J.-P. Valour, Y. Chevalier, Int. J. Pharm. 371 (2009) 56.
[5] W. Ramsden, Proc. R. Soc. London 72 (1903) 156.
[6] S. Simovic, C.A. Prestidge, Eur. J. Pharm. Biopharm. 67 (2007) 39.
[7] P.J. Colver, S.A.F. Bon, Chem. Mater. 19 (2007) 1537.
[8] S. Fujii, M. Okada, T. Furuzono, J. Colloid Interface Sci. 315 (2007) 287.
[9] Y. He, Mater. Lett. 59 (2005) 114.
[10] Q. Xiao, X. Tan, L. Ji, J. Xue, Synth. Met. 157 (2007) 784.
[11] S. Melle, M. Lask, G.G. Fuller, Langmuir 21 (2005) 2158.
[12] B.I. Yakobson, C.J. Brabec, J. Bernholc, Phys. Rev. Lett. 76 (1996) 2511.
[13] H. Wang, E.K. Hobbie, Langmuir 19 (2003) 3091.
[14] J. Hone, B. Batlogg, Z. Benes, A.T. Johnson, J.E. Fischer, Science 289 (2000) 1730.
[15] M.M. Gudarzi, F. Sharif, Soft Matter 7 (2011) 3432.
[16] W. Wang, E.D. Laird, Y. Gogotsi, C.Y. Li, Carbon 50 (2012) 1769.
[17] W. Zhai, G. Li, P. Yu, L. Yang, L. Mao, J. Phys. Chem. C 117 (2013) 15183.
[18] P. Xie, X. Ge, B. Fang, Z. Li, Y. Liang, C. Yang, Colloid Polym. Sci. 291 (2013) 1631.
[19] Y. He, F. Wu, X. Sun, R. Li, Y. Guo, C. Li, L. Zhang, F. Xing, W. Wang, J. Gao, ACS Appl. Mater. Interfaces 5 (2013) 4843.
[20] J. Kim, L.J. Cote, F. Kim, W. Yuan, K.R. Shull, J. Huang, J. Am. Chem. Soc. 132 (2010) 8180.
[21] G. Yin, Z. Zheng, H. Wang, Q. Du, H. Zhang, J. Colloid Interface Sci. 394 (2013) 192.
[22] F. Kim, L.J. Cote, J. Huang, Adv. Mater. 22 (2010) 1954.
[23] T.M. McCoy, M.J. Pottage, R.F. Tabor, J. Phys. Chem. C 118 (2014) 4529.
[24] S.Z. Moghaddam, S. Sabury, F. Sharif, RSC Adv. 4 (2014) 8711.
[25] M. Tang, X. Wang, F. Wu, Y. Liu, S. Zhang, X. Pang, X. Li, H. Qiu, Carbon 71 (2014) 238.
[26] R.H. Engel, S.J. Riggi, Nature 219 (1968) 856.
[27] P.A. Gresham, M. Barnett, S.V. Smith, R. Schneider, Nature 234 (1971) 149.
[28] S.S. Davis, L. Illum, I.M. Walker, Int. J. Pharm. 38 (1987) 133.

[29] J. Frelichowska, M.-A. Bolzinger, J.-P. Valour, H. Mouaziz, J. Pelletier, Y. Chevalier, Int. J. Pharm. 368 (2009) 7.
[30] F. Lachampt, A. Viout, G. Vanlerberghe, in: Google Patents, 1970.
[31] K. Miyazawa, I. Yajima, I. Kaneda, T. Yanaki, J. Soc. Cosmet. Chem. 51 (2000) 239.
[32] S. Matsumoto, Y. Ueda, Y. Kita, D. Yonezawa, Agric. Biol. Chem. 42 (1978) 739.
[33] A. Kaiser, T. Liu, W. Richtering, A.M. Schmidt, Langmuir 25 (2009) 7335.
[34] Q. Lan, C. Liu, F. Yang, S. Liu, J. Xu, D. Sun, J. Colloid Interface Sci. 310 (2007) 260.
[35] J. Zhou, X. Qiao, B.P. Binks, K. Sun, M. Bai, Y. Li, Y. Liu, Langmuir 27 (2011) 3308.
[36] B.P. Binks, Curr. Opin. Colloid Interface Sci. 7 (2002) 21.
[37] U.T. Gonzenbach, A.R. Studart, E. Tervoort, L.J. Gauckler, Angew. Chem. Int. Ed. 45 (2006) 3526.
[38] T.N. Hunter, R.J. Pugh, G.V. Franks, G.J. Jameson, Adv. Colloid Interface Sci. 137 (2008) 57.
[39] O.D. Velev, B.G. Prevo, K.H. Bhatt, Nature 426 (2003) 515.
[40] K.P. Velikov, O.D. Velev, Wiley-VCH Publ., Weinheim, 2007, p. 277.
[41] A. Cervantes Martinez, E. Rio, G. Delon, A. Saint-Jalmes, D. Langevin, B.P. Binks, Soft Matter 4 (2008) 1531.
[42] S. Kim, H. Barraza, O.D. Velev, J. Mater. Chem. 19 (2009) 7043.
[43] R. Klajn, K.J.M. Bishop, B.A. Grzybowski, Proc. Natl. Acad. Sci. 104 (2007) 10305.
[44] R. Klajn, J.F. Stoddart, B.A. Grzybowski, Chem. Soc. Rev. 39 (2010) 2203.
[45] A. Salonen, D. Langevin, P. Perrin, Soft Matter 6 (2010) 5308.
[46] H.A. Wege, S. Kim, V.N. Paunov, Q. Zhong, O.D. Velev, Langmuir 24 (2008) 9245.
[47] S. Lam, E. Blanco, S.K. Smoukov, K.P. Velikov, O.D. Velev, J. Am. Chem. Soc. 133 (2011) 13856.
[48] P. Aussillous, D. Quere, Nature 411 (2001) 924.
[49] P. Aussillous, D. Quéré, Phys. Eng. Sci. 462 (2006) 973.
[50] E. Bormashenko, R. Pogreb, Y. Bormashenko, A. Musin, T. Stein, Langmuir 24 (2008) 12119.
[51] L. Gao, T.J. McCarthy, Langmuir 23 (2007) 10445.
[52] P.H. Hoang, H. Park, D.-P. Kim, J. Am. Chem. Soc. 133 (2011) 14765.
[53] X. Hong, X. Gao, L. Jiang, J. Am. Chem. Soc. 129 (2007) 1478.
[54] M. Joanicot, A. Ajdari, Science 309 (2005) 887.
[55] K.T. Kotz, Y. Gu, G.W. Faris, J. Am. Chem. Soc. 127 (2005) 5736.
[56] L. Mahadevan, Y. Pomeau, Phys. Fluids 11 (1999) 2449.
[57] G. McHale, M.I. Newton, Soft Matter 7 (2011) 5473.
[58] H. Song, D.L. Chen, R.F. Ismagilov, Angew. Chem. Int. Ed. 45 (2006) 7336.
[59] J. Tian, T. Arbatan, X. Li, W. Shen, Chem. Commun. 46 (2010) 4734.
[60] Y. Xue, H. Wang, Y. Zhao, L. Dai, L. Feng, X. Wang, T. Lin, Adv. Mater. 22 (2010) 4814.
[61] Y. Zhao, J. Fang, H. Wang, X. Wang, T. Lin, Adv. Mater. 22 (2010) 707.
[62] A.B. Theberge, F. Courtois, Y. Schaerli, M. Fischlechner, C. Abell, F. Hollfelder, W.T.S. Huck, Angew. Chem. Int. Ed. 49 (2010) 5846.
[63] W.S. Hummers, R.E. Offeman, J. Am. Chem. Soc. 80 (1958) 1339.
[64] J. Shen, M. Shi, H. Ma, B. Yan, N. Li, M. Ye, Mater. Res. Bull. 46 (2011) 2077.
[65] H.-J. Shin, K.K. Kim, A. Benayad, S.-M. Yoon, H.K. Park, I.-S. Jung, M.H. Jin, H.-K. Jeong, J.M. Kim, J.-Y. Choi, Y.H. Lee, Adv. Funct. Mater. 19 (2009) 1987.
[66] S. Zhang, L. Zhu, H. Song, X. Chen, B. Wu, J. Zhou, F. Wang, J. Mater. Chem. 22 (2012) 22150.
[67] D.C. Marcano, D.V. Kosynkin, J.M. Berlin, A. Sinitskii, Z. Sun, A. Slesarev, L.B. Alemany, W. Lu, J.M. Tour, ACS Nano 4 (2010) 4806.
[68] J. Shen, Y. Hu, M. Shi, N. Li, H. Ma, M. Ye, J. Phys. Chem. C 114 (2010) 1498.
[69] A.C. Ferrari, J.C. Meyer, V. Scardaci, C. Casiraghi, M. Lazzeri, F. Mauri, S. Piscanec, D. Jiang, K.S. Novoselov, S. Roth, A.K. Geim, Phys. Rev. Lett. 97 (2006) 187401.
[70] K.N. Kudin, B. Ozbas, H.C. Schniepp, R.K. Prud'homme, I.A. Aksay, R. Car, Nano Lett. 8 (2007) 36.
[71] A. Chunder, J. Liu, L. Zhai, Macromol. Rapid Commun. 31 (2010) 380.
[72] A. Jorio, E.H.M. Ferreira, M.V.O. Moutinho, F. Stavale, C.A. Achete, R.B. Capaz, Phys. Status Solidi (b) 247 (2010) 2980.
[73] H.-M. Ju, S.-H. Choi, S.H. Huh, J. Korean Phys. Soc. 57 (2010) 1649.
[74] V. Loryuenyong, K. Totepvimarn, P. Eimburanapravat, W. Boonchompoo, A. Buasri, Adv. Mater. Sci. Eng. 2013 (2013) 5.
[75] W. Wu, Q. He, C. Jiang, Nanoscale Res. Lett. 3 (2008) 397.
[76] A.L. Flint, L.E. Flint, in: J.H. Dane, C.G. Topp (Eds.), Methods of Soil Analysis: Part 4 Physical Methods, Soil Science Society of America, 2002, p. 229.
[77] G.Z. Kyzas, E.A. Deliyanni, K.A. Matis, J. Chem. Technol. Biotechnol. 89 (2014) 196.
[78] J. Wang, T. Tsuzuki, B. Tang, X. Hou, L. Sun, X. Wang, ACS Appl. Mater. Interfaces 4 (2012) 3084.